ASYMPTOTIC APPROXIMANT FOR THE FALKNER–SKAN BOUNDARY LAYER EQUATION

by E. R. BELDEN *and* Z. A. DICKMAN

(*Department of Chemical Engineering, Rochester Institute of Technology, Rochester, NY* 14623, *USA*)

S. J. WEINSTEIN

(*Department of Chemical Engineering, Rochester Institute of Technology, Rochester, NY 14623, USA and School of Mathematical Sciences, Rochester Institute of Technology, Rochester, NY 14623, USA*)

A. D. ARCHIBEE

(*Department of Mechanical Engineering, Rochester Institute of Technology, Rochester, NY* 14623, *USA*)

E. BURROUGHS *and* N. S. BARLOW[†]

(*School of Mathematical Sciences, Rochester Institute of Technology, Rochester, NY* 14623, *USA*)

[Received 15 July 2019. Revise 7 October 2019. Accepted 8 October 2019]

Summary

We demonstrate that the asymptotic approximant applied to the Blasius boundary layer flow over a flat plat (Barlow *et al.*, *Q. J. Mech. Appl. Math.* **70** (2017) 21–48.) yields accurate analytic closed-form solutions to the Falkner–Skan boundary layer equation for flow over a wedge having angle $\beta\pi/2$ to the horizontal. A wide range of wedge angles satisfying $\beta \in [-0.198837735, 1]$ are considered, and the previously established non-unique solutions for $\beta < 0$ having positive and negative shear rates along the wedge are accurately represented. The approximant is used to determine the singularities in the complex plane that prescribe the radius of convergence of the power series solution to the Falkner–Skan equation. An attractive feature of the approximant is that it may be constructed quickly by recursion compared with traditional Padé approximants that require a matrix inversion. The accuracy of the approximant is verified by numerical solutions, and benchmark numerical values are obtained that characterize the asymptotic behavior of the Falkner–Skan solution at large distances from the wedge.

1. Introduction

The Falkner–Skan equation describes boundary layer flow over a wedge of angle $\beta\pi/2$ to the horizontal that is driven by an external pressure gradient predicted from potential flow (see Fig. 1). The equation also applies to regimes where the pressure gradient opposes the flow when $\beta < 0$ (Fig. 1(c) and (d)) for which boundary layer separation may occur. Through a similarity transform, the governing two-dimensional boundary layer equations can be written as a nonlinear ordinary

[†] <nsbsma@rit.edu>

Q. Jl Mech. Appl. Math, Vol. 73. No. 1 © The Author, 2020. Published by Oxford University Press; all rights reserved. For Permissions, please email: journals.permissions@oup.com. Advance Access publication 10 February 2020. doi:10.1093/qjmam/hbz021

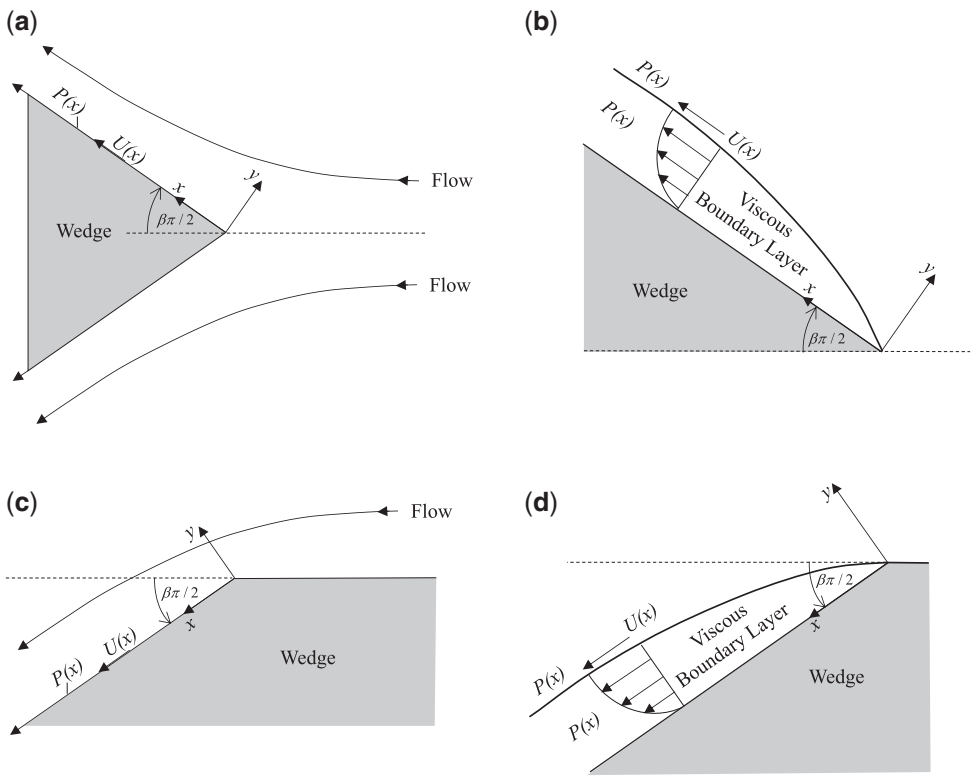

Fig. 1 Geometry of flow over a wedge showing potential flow and viscous boundary layer regions. (a) Domain for the potential flow solution for $\beta > 0$, from which the nonzero velocity $U(x)$ and associated Bernouli pressure $P(x)$ along $y = 0$ is extracted. (b) Domain for the thin viscous boundary layer (Falkner–Skan problem) that is driven by the potential flow solutions for $U(x)$ and $P(x)$. There are no pressure variations in the y-direction. On the length scale of figure (a), the boundary layer cannot be observed. The analogous wedge configuration for $\beta < 0$ are shown in figures (c) and (d).

differential equation (ODE) system for the dimensionless stream function, f, as a function of a similarity variable $\eta(x, y)$ (**1**):

$$f''' + ff'' + \beta(1 - f'^2) = 0$$
$$f(0) = 0, f'(0) = 0, f'(\infty) = 1. \tag{1.1}$$

Once (1.1) is solved for $f(\eta)$, the dimensional stream function, $\psi(x, y)$, may be extracted as (**1**)

$$\eta = y\sqrt{\frac{m+1}{2}\frac{U}{\nu x}} \tag{1.2}$$

$$\psi(x, y) = f(\eta)\sqrt{\frac{2\nu U x}{m+1}},$$

where x and y are coordinates along and perpendicular to the wedge surface (see Fig. 1), $m = \beta/(2-\beta)$, ν is kinematic viscosity and $U = U(x)$ is the velocity at the wedge surface determined from potential flow, as indicated in Fig. 1. Although a power series solution can be found for (1.1), it diverges at a finite value of η for all physical values of wedge angle β. The lack of an exact analytical solution has necessitated several numerical (**2**–**8**) and approximate analytical (**9**–**11**) solution approaches to the system (1.1). Here, we implement the recent method of asymptotic approximants to analytically continue the power series solution, and thereby construct a highly accurate closed-form solution to (1.1).

Asymptotic approximants are used to sum divergent series and may be constructed when asymptotic behaviors are known in two different regions of a domain; implementation details are given in (**12**–**17**). The method is a generalization of two well-known mathematical techniques: asymptotic matching and Padé approximants (**18**). Whereas asymptotic matching leads to a single expression that combines two *overlapping* asymptotic expansions, asymptotic approximants do not require that the two series overlap; if the two series diverge before overlap, an asymptotic approximant has the ability to analytically continue each series and accurately fill in the gap between them. Two-point Padés and other generalizations of Padé approximants have also been used to accomplish this task (**19**–**21**). In the same way as Padé approximants, asymptotic approximants are constructed such that the series expansion of the approximant about a given point is the same as that of the true expansion about that point. However, whereas Padé approximants are restricted to rational functions and thus have a specific asymptotic behavior about a chosen expansion point, asymptotic approximants are tailor-made to have the correct behavior in both regions of the domain. For example, asymptotic approximants are shown to accurately describe the light trajectory around a Kerr black hole (**16**, **17**) by incorporating the correct logarithmic behavior near the black hole; a Padé is incapable of representing such behavior efficiently. Asymptotic approximants are used to construct accurate solutions for boundary layer flows over a stationary flat plate (the Blasius problem) and for a flat plate moving through a stationary fluid (the Sakiadis problem) (**15**). The Blasius approximant uses a power series expansion about $\eta = 0$ and the leading-order behavior as $\eta \to \infty$; the full asymptotic behavior in this latter regime is not needed to obtain a highly accurate solution. The leading-order $\eta \to \infty$ behavior of Blasius is exactly the same as that for the Falkner–Skan problem (1.1) for flow over a wedge. Thus the asymptotic approximant used in (**15**) for the Blasius problem may be applied to the Falkner–Skan equation. In this article, we construct a highly accurate approximant in which all coefficients are determined recursively (that is, they do not require a matrix inversion), and through which the location of complex singularities that lead to series divergence are identified.

Although accurate numerical solutions to nonlinear ODEs such as (1.1) are easily obtained today on a modest computer, it can be advantageous to utilize an analytic form provided by an approximant. Analytic forms enable highly resolved solutions on domains of arbitrary length to be obtained without (a) interpolation or extrapolation of the numerical solution or (b) re-running the numerical solution at higher computational cost. Additionally, analytic solutions preserve accuracy when integration or differentiation is required to obtain auxiliary properties of the flow field. The main goal here, however, is to advance the method of asymptotic approximants by demonstrating that the method disclosed in previous work (**12**–**17**) may be applied to (1.1). The ability of the approximant to capture the full range of solutions (as wedge angle is varied), and the accuracy of auxiliary properties obtained using the approximant, are examined as well.

The article is organized as follows. In section 2, the series solution of (1.1) and numerically obtained asymptotic properties are provided as a function of wedge angle. The Blasius asymptotic approximant of (**15**) is applied to the Falkner–Skan equation in section 3; it is validated against

numerical solutions for key values of wedge angle. The Blasius-type approximant is found to be accurate for positive and negative shear rates at the wedge surface over a significant range of wedge angles—the range of β encompasses all physical configurations for which there is no boundary layer separation. An alternative asymptotic approximant is introduced to handle non-monotonic solutions to the Falkner–Skan equation that occur over a small range of negative shear rates at the wedge surface for $\beta < 0$. In section 3.1, the Blasius-type approximant is used to extract the radius of convergence of the Falkner–Skan series as a function of wedge angle; to the authors' knowledge, this is the first time this dependence has been disclosed. Concluding remarks are made in section 4.

2. Asymptotic properties and series expansion of the Falkner–Skan equation

Solutions to the Falkner–Skan equation system (1.1) are found for a given flow by fixing the parameter β, which is related to the wedge angle shown in Fig. 1. Note that this parameter incorporates the effect of wedge angle on the potential flow that drives the fluid motion in the boundary layer. Although (1.1) is a boundary value problem, a series solution may be generated if the infinity boundary condition is relaxed, and the dimensionless velocity gradient at the wedge surface, $\kappa(\beta)$, is applied at $\eta = 0$ as

$$f''(0) = \kappa(\beta). \tag{2.1}$$

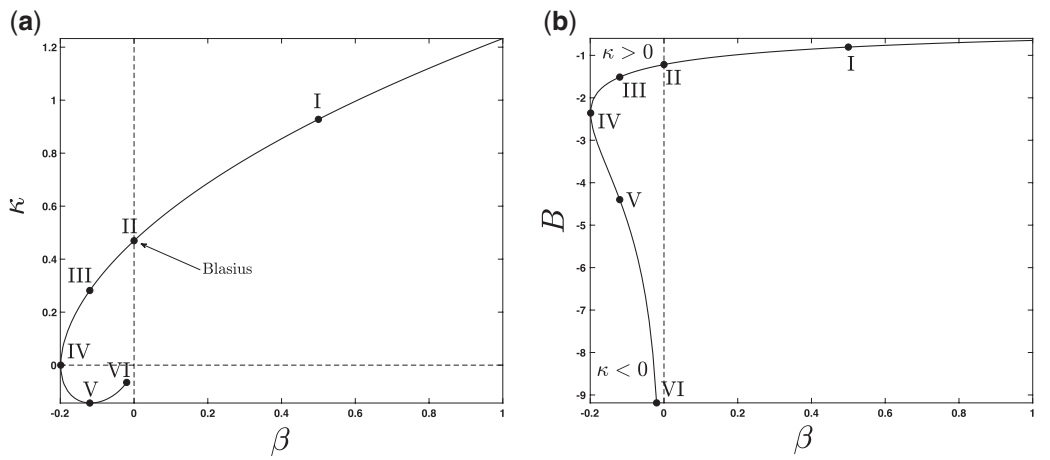

Fig. 2 Solution properties as a function of the wedge angle parameter, β, obtained from the Falkner–Skan system (1.1). (a) Dimensionless velocity gradient, $\kappa = f''(0)$, used to construct the series expansion (2.2). (b) Asymptotic constant B defined according to (2.3). The constants κ and B are determined numerically using the shooting method of (**2**) with marching done using the fourth-order Runge–Kutta method with a step size of 10^{-4}. Specific values of (β, κ, B) associated with the roman numerals in the plots are as follows: I. (0.5, 0.927680039836653, −0.804548615), II. (0, 0.469599988361, −1.21678062) III. (−0.12, 0.28176052424, −1.511343148) IV. (−0.198837735, 0, −2.359), V. (−0.12, −0.1429351943576, −4.3989990662) and VI. (−0.02, −0.065168585542904, −9.18639214). Convergence has been established to within the digits reported above by successively increasing the domain length ($\eta \in [0, L]$, L=10, 20, 30, 40) of the shooting method. A tabulated version of this data is provided in Supplementary Data.

Note that the function $\kappa(\beta)$ in (2.1) is determined such that the $\eta \to \infty$ boundary condition in (1.1) is applied and is typically determined numerically. Figure 2(a) shows the dependence of κ on the wedge angle parameter β; the figure is constructed by implementing the shooting method of (**2**). Key values in Fig. 2(a) are as follows. When $\beta = 0$ (point II in Fig. 2(a)), there is no pressure gradient in the physical system, and the system (1.1) describes the classical Blasius problem for flow along a flat plate[‡]. When $\kappa = 0$ (Point IV in Fig. 2(a), $\beta \approx -0.1988$), the velocity gradient along the wedge is zero, and this condition corresponds to the onset of boundary layer separation (**1**). As shown in Fig. 2(a), there are multiple solutions to (1.1) for $\beta < 0$. Negative values of κ (for example, Points V and VI in Fig. 2(a)) correspond to solutions of (1.1) that contain a region where f' is negative before eventually switching sign to tend towards the asymptotic behavior $f' \to 1$, given in (1.1); this is referred to as a region of 'reversed flow' by Stewartson (**24**).

The series solution to (1.1) may be obtained (**25**) as

$$f = \sum_{n=0}^{\infty} a_n \eta^n, \tag{2.2a}$$

where

$$a_{n+3} = \frac{\sum_{j=0}^{n} \beta(j+1)(n-j+1)a(j+1)a(n-j+1) - (j+1)(j+2)a_{j+2}a_{n-j}}{(n+1)(n+2)(n+3)}. \tag{2.2b}$$

The recursion above requires knowledge of the first three coefficients in order to generate the full series. The first two coefficients $a_0 = f(0)$=0 and $a_1 = f'(0)$=0 are given by the first two boundary conditions in (1.1). The third coefficient $a_2 = f''(0)/2 = \kappa/2$ is taken from the numerical solution described above and shown in Fig. 2(a). As evidenced by Figs 3(a)–7(a), the utility of the series (2.2) is limited for all values of β as it has a finite radius of convergence. The dependence of the radius of convergence on β is investigated in section (3.1).

The far-field condition $f'(\infty) = 1$ appearing in (1.1) holds true for all wedge angles β, as does the admission of an integration constant in this limit, such that the leading-order asymptotic behavior may be written as (**26**)

$$\lim_{\eta \to \infty} (f - \eta) \equiv B(\beta), \tag{2.3}$$

where B[§] is a function of wedge angle β; the dependence is shown in Fig. 2(b). Both Fig. 2(a) and (b) are constructed by implementing the numerical shooting method of (**2**), replacing ∞ in (2.3) with a finite domain length L, calculating κ and $B \approx [f(\eta = L) - L]$, and recomputing the numerical solution for successively increased L until κ and B are converged to within the tolerance reported in the figure caption. Although presented in Fig. 2 using newly generated numerical solutions, the functionality of both κ and B on β has long been known (**24**).

[‡] The common form of the Blasius equation includes a coefficient of 1/2 in front of the ff'' term, as a result of omitting the factor of 2 in the denominator of (1.2) when deriving (1.1) from the governing equations with $\beta = 0$ (**1**). A ramification of this is that the values reported here are $\sqrt{2}\times$ the literature value of $\kappa = 0.3320573362152$ and $1/\sqrt{2}\times$ the literature value of $B = -1.72078765752$ (**22**, **23**).

[§] The parameter B is the negative of the *displacement thickness* defined in terms of the similarity variables as $\delta_1 = \int_0^\infty (1 - f')\, d\eta$ (**24**). In this article, we define the quantity B such that (2.3) is consistent with the notation typically used for the Blasius problem ($\beta = 0$) (**22**).

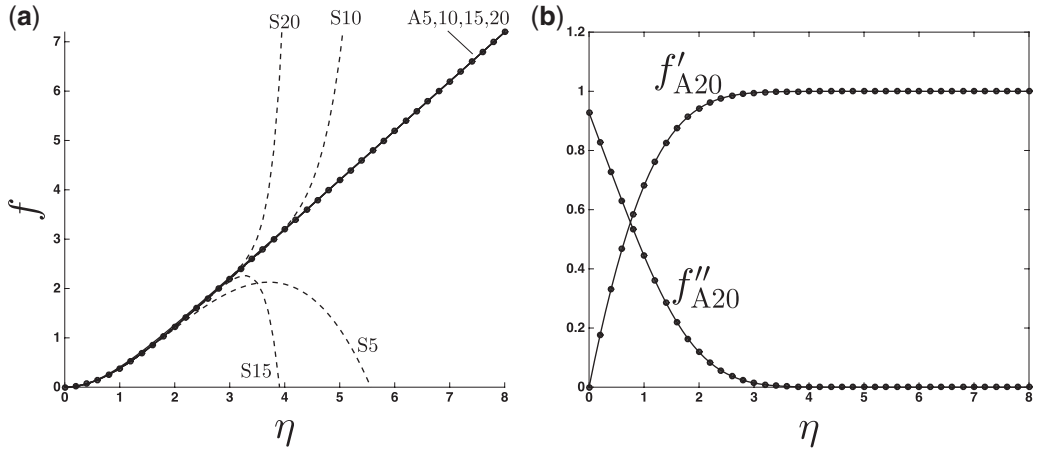

Fig. 3 (a) The N-term series (2.2) labeled SN and approximant (3.1) labeled AN compared with numerical solution (•). (b) Derivatives of approximant (3.1) for $N = 20$. Data shown here corresponds to conditions at point I in Fig. 2 ($\beta = 0.5$, $\kappa = 0.927680039836653$).

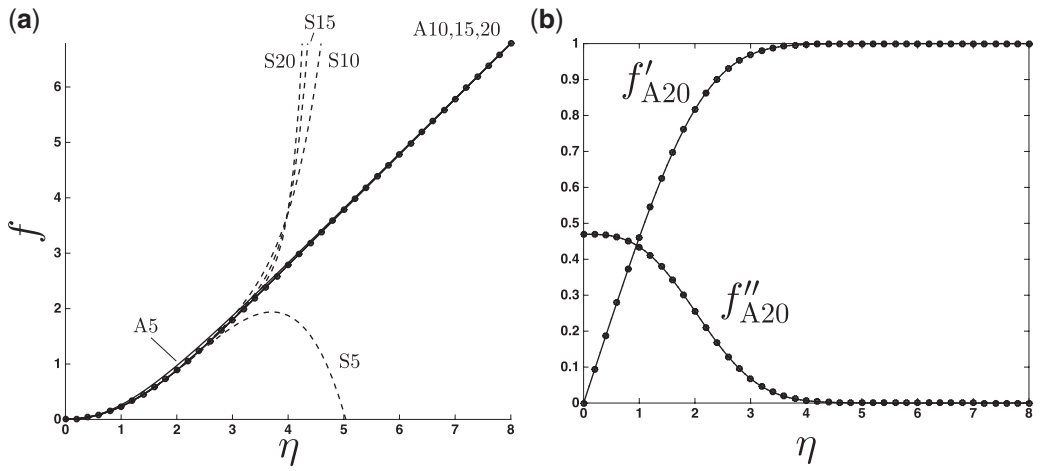

Fig. 4 (a) The N-term series (2.2) labeled SN and approximant (3.1) labeled AN compared with numerical solution (•). (b) Derivatives of approximant (3.1) for N=20. Data shown here corresponds to conditions at point II in Fig. 2 ($\beta = 0$, $\kappa = 0.469599988361$). These results correspond to the classical boundary layer solution of Blasius.

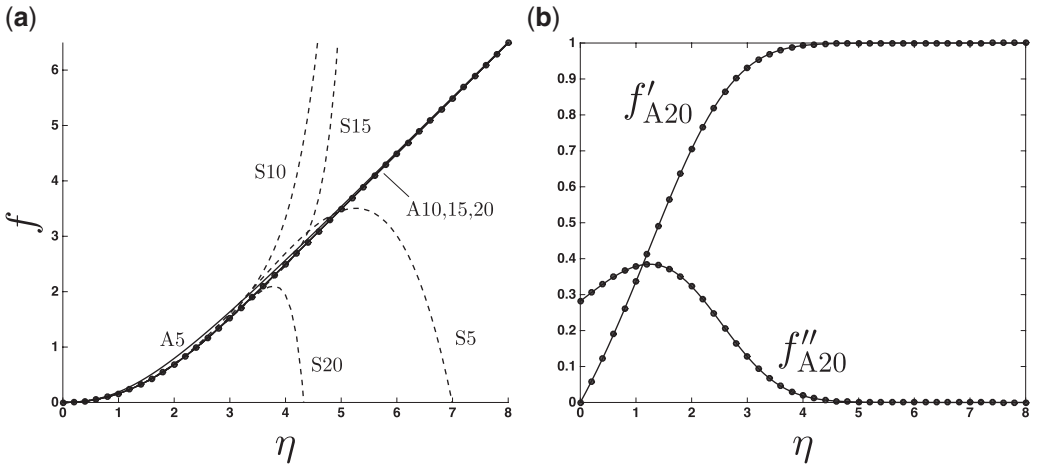

Fig. 5 (a) The N-term series (2.2) labeled SN and approximant (3.1) labeled AN compared with numerical solution (•). (b) Derivatives of approximant (3.1) for $N = 20$. Data shown here corresponds to conditions at point III in Fig. 2 ($\beta = -0.12, \kappa = 0.28176052424$). This solution is not unique—there is another solution for the same value of β corresponding to point V in Fig. 2, as shown in Fig. 7.

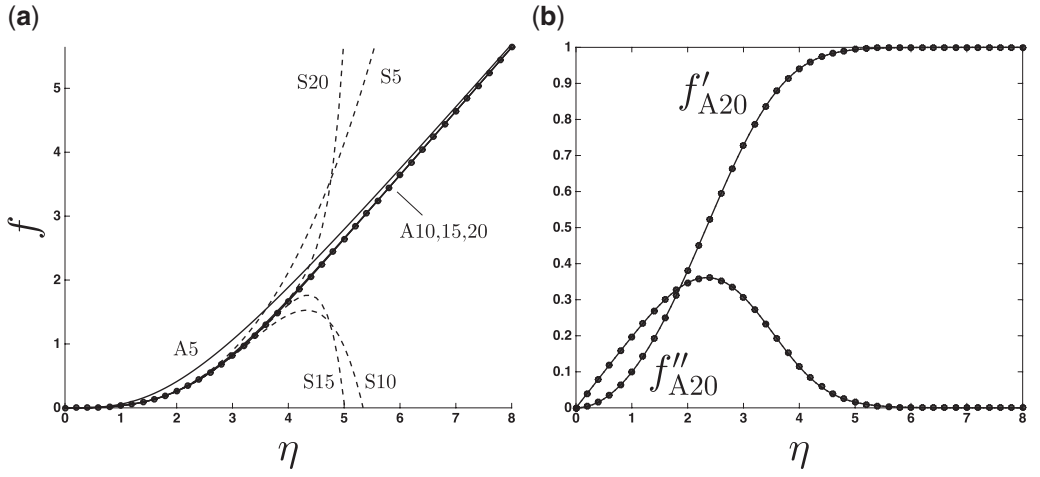

Fig. 6 (a) The N-term series (2.2) labeled SN and approximant (3.1) labeled AN compared with numerical solution (•). (b) Derivatives of approximant (3.1) for N=20. Data shown here corresponds to conditions at point IV in Fig. 2 ($\beta = -0.198837735, \kappa = 0$). These results correspond to the conditions at the onset of boundary layer separation, for which the shear rate at wedge surface is zero.

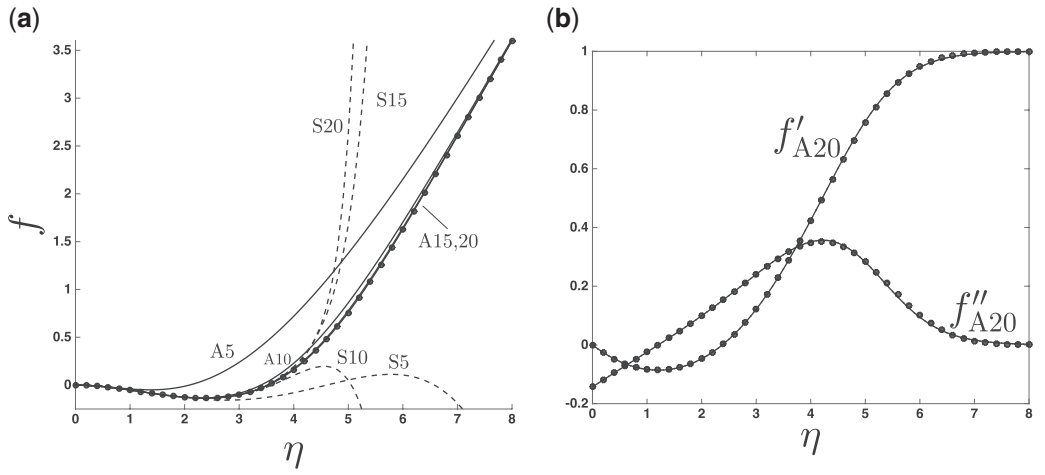

Fig. 7 (a) The N-term series (2.2) labeled SN and approximant (3.1) labeled AN compared with numerical solution (•). (b) Derivatives of approximant (3.1) for N=20. Data shown here corresponds to conditions at point V in Fig. 2 ($\beta = -0.12$, $\kappa = -0.1429351943576$). This solution is not unique – there is another solution for the same value of β corresponding to point III in Fig. 2, as shown in Fig. 5.

3. Asymptotic approximant

The divergence of the Falkner–Skan series (2.2) demonstrated in Figs 3(a)–7(a) is overcome using the method of asymptotic approximants, which constrains the analytic continuation of the series via an asymptotic behavior away from the point of expansion (**15**). An approximant that satisfies the $\eta \to \infty$ behavior (2.3) is given as

$$f_A = \eta + B - B\left(1 + \sum_{n=1}^{N} A_n\, \eta^n\right)^{-1}, \tag{3.1a}$$

where the A_n coefficients are chosen such that the expansion of (3.1a) about $\eta = 0$ is exactly (2.2) up to Nth order. Note that the above form is not a Padé approximant for f, in that if one combines the terms of (3.1a) through a common denominator, the coefficients of the numerator will have an explicit dependence on those in the denominator—this is not the case for standard Padés. That said, (3.1a) may be formulated as a Padé approximant for the quantity $(f - \eta - B)/B$. The form of the approximant (3.1a) is used in (**15**) for $\beta = 0$ to generate accurate solutions of the Blasius boundary layer problem for flow over a flat plate.

A recursion for the coefficients A_n in (3.1a) is obtained as follows. The N-term Taylor expansion of (3.1a) about $\eta = 0$ is set equal to the N-term truncation of (2.2). Then, taking the limit $N \to \infty$, and re-arranging yields

$$\sum_{n=0}^{\infty} \tilde{a}_n \eta^n = -B\left(\sum_{n=0}^{\infty} A_n \eta^n\right)^{-1},$$

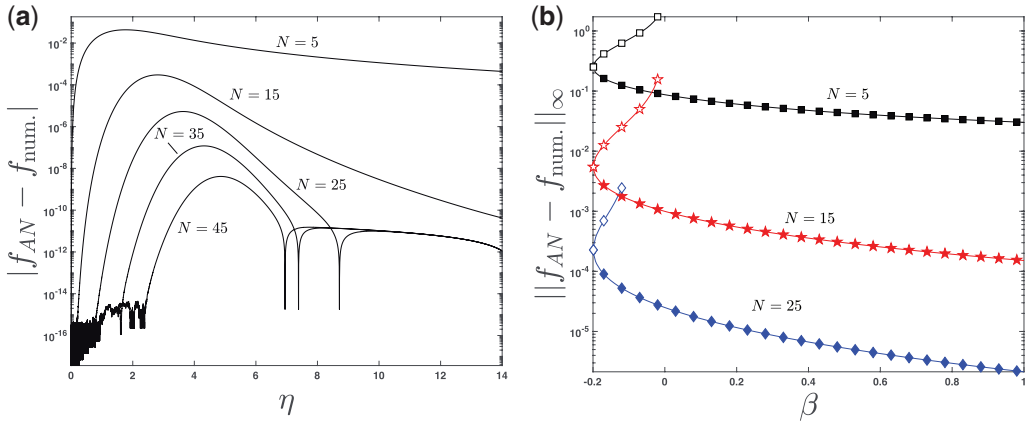

Fig. 8 Error associated with approximant (3.1), measured against numerical solutions with truncation error of $O(10^{-16})$. (a) Absolute error in approximant (3.1) for $\beta = 0.5$. (b) Infinity norm (taken over $0 \leq \eta \leq 14$) of the absolute error associated with the approximant for $-0.198837735 \leq \beta \leq 2$. The multivalued solutions for $\beta < 0$ are represented here; the filled and open symbols correspond to $\kappa > 0$ and $\kappa < 0$ solutions, respectively.

where (noting that $a_0 = a_1 = 0$) $\tilde{a}_0 = -B, \tilde{a}_1 = -1, \tilde{a}_2 = a_2 = \kappa/2$ and $\tilde{a}_{j>2} = a_j$ (given by (2.2b)). Multiplying both sides of the above by the A_n series and applying the well-known identity for the Cauchy product of two series (**27**), the expression becomes

$$\sum_{n=0}^{\infty} \left(\sum_{j=0}^{n} \tilde{a}_j A_{n-j} \right) \eta^n = -B.$$

Noting that $\tilde{a}_0 = -B$, the above can be separated as

$$-BA_0 + \sum_{n=1}^{\infty} \left(-BA_n + \sum_{j=1}^{n} \tilde{a}_j \, A_{n-j} \right) \eta^n = -B.$$

Equating like terms of η^0 and $\eta^{n\neq 0}$ in the expression above, we arrive at the following

$$A_0 = 1,$$
$$A_{n>0} = \frac{1}{B} \sum_{j=1}^{n} \tilde{a}_j \, A_{n-j}, \;\; \tilde{a}_1 = -1, \;\; \tilde{a}_{j>1} = a_j, \tag{3.1b}$$

such that now all A_n coefficients may be computed recursively. Note that the result (3.1b) is identical to that provided in previous work (**15**) for the Blasius solution ($\beta = 0$), but here we provide the intermediate steps for purposes of clarity.

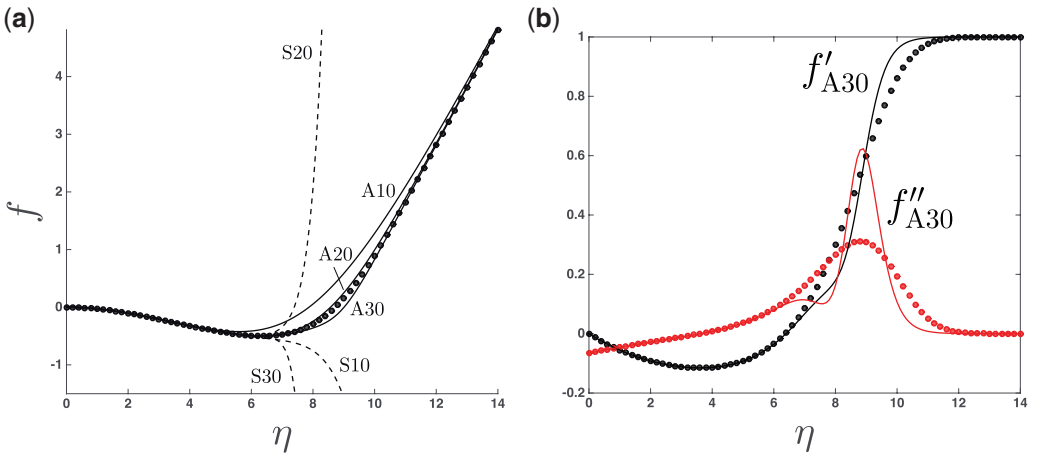

Fig. 9 (a) The N-term series (2.2) labeled SN and approximant (3.1) labeled AN compared with numerical solution (•). (b) Derivatives of approximant (3.1) for $N = 30$. Data shown here corresponds to conditions at point VI in Fig. 2 ($\beta = -0.02$, $\kappa = -0.065168585542904$).

The approximant (3.1) is compared with the series and numerical solutions in Figs 3–7 for the specific values of β enumerated as I through V in Fig. 2 (case VI is discussed separately). As is evident in the figures, curves for f_A approach a final curve shape as N increases. In fact, a key property of a valid approximant is that, upon increasing the order N, a convergent sequence of approximants is obtained in the sense of Cauchy. The justification for the choice of approximant form is this convergent behavior. Since all derivatives of the approximant can be computed exactly, it is not surprising that derivatives of the approximant are in excellent agreement with the numerical solution, as shown in Figs 3(b)–7(b).

Convergence of approximant (3.1) is shown on a more sensitive scale in Fig. 8a for $\beta = 0.5$, where the absolute error between the approximant and the numerical solution is shown for different N values. The convergence behavior shown in the figure is representative of other β values within the range examined here. The infinity norm of the error for $\eta \in [0, 14]$ is shown in Fig. 8b over the full range of β. For the cases of positive κ (filled symbols of Fig. 8b), convergence of approximant (3.1) is established for all β, such that accurate solutions are obtained. For the cases of negative κ (open symbols of Fig. 8b), convergence is apparent but is increasingly limited as $\beta \to 0^-$. Note from Fig. 8b that the overall error increases in this limit, and approximant (3.1) becomes worse at representing the solution. This limited convergence is demonstrated in Fig. 9 for $\beta = -0.02$ ($\kappa < 0$, point VI in Fig. 2), where approximant (3.1) is shown to poorly represent the solution for intermediate values of η; an improvement is discussed below.

The monotonic or nearly monotonic solutions in $f(\eta)$ shown in Figs 3–7 (representing cases I through V in Fig. 2) enable the simple form of approximant (3.1) to provide accurate solutions over the physical domain, from $\eta = 0$ towards 'large' η such that $f' \to 1$. As β approaches 0 from the left for $\kappa < 0$, $f(\eta)$ becomes less monotonic and a minima manifests prior to reaching the $f' \to 1$ large η behavior, as shown in Fig. 9 for $\beta = -0.02$ (point VI in Fig. 2). As mentioned above, approximant (3.1) is incapable of correctly resolving this minima in $f(\eta)$. To allow for more flexible

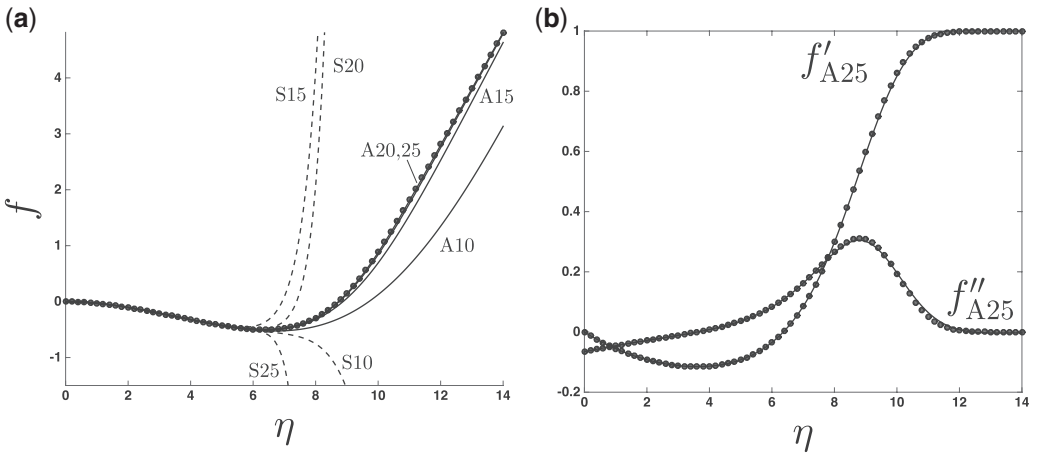

Fig. 10 (a) The N-term series (2.2) labeled SN and approximant (3.2) labeled AN compared with numerical solution (•). (b) Derivatives of approximant (3.2) for $N = 25$. Data shown here corresponds to conditions at point VI in Fig. 2 ($\beta = -0.02$, $\kappa = -0.065168585542904$).

curve shapes, the approximant is adjusted to have a cubic form in its numerator as follows:

$$f_A = \eta + B - B\left[\frac{A_0 + A_1\eta + A_2\eta^2 + A_3\eta^3}{1 + \sum_{n=1}^{N-3} d_n\eta^n}\right], \quad N > 3. \tag{3.2}$$

Like (3.1), approximant (3.2) satisfies the large η behavior (2.3) by construction. The unknown coefficients $A_0 \ldots A_3$ and d_n in (3.2) are chosen such that the expansion of (3.2) about η=0 is equal to the series given by (2.2) to order N. Note that the term in square brackets in (3.2) is a $[3/N-3]$ Padé approximant, for which solvers are readily available (**28**) to handle the required matrix inversion. One may compute the $A_0 \ldots A_3$ and d_n coefficients by isolating the bracketed term of (3.2) onto one side of the equation and finding the $[3/N-3]$ Padé for the power series $1 + \left(\eta - \sum_{n=0}^{N} a_n\eta^n\right)/B$. As before, the constants κ and B are taken from the numerical results shown in Fig. 2 and are inputs to the approximant. Figure 10 shows the convergence of approximant (3.2) applied to $\beta = -0.02$ ($\kappa < 0$, point VI in Fig. 2), and demonstrates a significant improvement over approximant (3.1) (see Fig. 9 for comparison). Note that, although a Padé solver can be used, (3.2) is not a standard Padé as they are defined today—it is a Padé as it was originally intended by Baker and Gammel (**29**), constructed such that it is consistent with the correct $\eta \to \infty$ limit.

Although an improvement is found using approximant (3.2) over the simpler approximant (3.1) for the cases of negative shear and small β, for all other β values (including those that are physically relevant), both approximants perform equally well. Approximant (3.1), however, is easier to compute, as it is based solely on recursion.

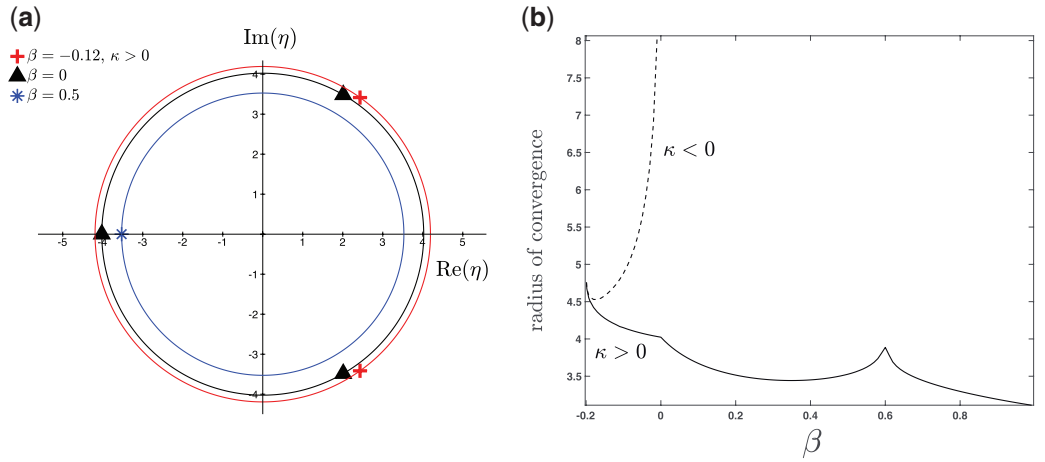

Fig. 11 (a) Location of singularities that limit convergence of the Falkner–Skan series (2.2), shown for three values of β. (b) Radius of convergence of (2.2); a tabulated version of this curve is provided in Supplementary Data.

3.1 *Complex singularities that limit convergence of power series solution (2.2)*

The power series result (2.2) is an exact representation of the solution to (1.1) within its radius of convergence. As there is no exact solution to (1.1), the radius of convergence must be extracted by examining successive terms in the power series using standard methods such as the ratio test (**30**). Alternatively, as has been done using Padé approximants (**31**, **32**), the asymptotic approximant (3.1) may be used to determine the location of these singularities and the radius of convergence of the series. The radius itself is set from the singularities closest to $\eta = 0$ in the solution of (1.1) when viewed in the complex plane; it follows, then, that the roots of the denominator of the approximant (3.1a) should be examined. Here, we increase the number of terms in the A_n series in the denominator of (3.1a) and obtain convergent solutions for the roots nearest to $\eta = 0$. Figure 11(a) provides results corresponding to three different values of β. Roots for $\beta = 0$ lie on the negative real axis, the first quadrant, and the fourth quadrant of the complex plane, and yield a radius of convergence of approximately 4.024 in agreement with Boyd (**22**, **33**)[‖]. For $0 < \beta < 0.6$, the root structure changes, as instead only one singularity appears that sets the circle convergence, lying on the negative real axis[¶], as shown in Fig. 11(a) for $\beta = 0.5$. For $\beta < 0$ ($\kappa > 0$ branch) there are a pair of singularities that set the circle of convergence, shown in Fig. 11(a) for $\beta = -0.12$ ($\kappa > 0$); this singularity orientation persists up until separation ($\beta = -0.199$). Outside of these ranges, for $\beta > -0.199$ ($\kappa < 0$) and $\beta > 0.6$, estimates for the roots using the approximant do not converge with increasing N. However, even when the roots do not converge, the singularities move in such a way that their distance from $\eta = 0$ does converge for all β excluding $0.5 < \beta < 0.6$; over this limited range of β,

[‖] As a result of using a different similarity variable, the value reported in (**22**, **33**) is $\sqrt{2}\times$ our value (see footnote † in section 2).

[¶] For $0.5 < \beta < 0.6$, the singularity location (orientation and radius) does not converge using (3.1). However, the series terms eventually alternate sign at higher-order, indicating that the closest singularity lies on the negative real axis.

the ratio-test provides an accurate radius of convergence—thus, the radius of convergence of (2.2) may be determined. Figure 11(b) shows the dependence of radius of convergence on β. Note that, although Fig. 11(b) indicates an apparent infinite radius of convergence for $\beta \to 0^-$ ($\kappa < 0$), Figs 7 and 9 (typical of other cases) show that the local minima in the $f(\eta)$ curve roughly tracks along with the radius of convergence and is pushed farther out as β becomes small. Thus, although the radius of convergence increases for smaller β past separation ($\kappa < 0$), the asymptotic behavior ($f' \to 1$) is never captured by the series.

4. Conclusions

Asymptotic approximants provide nearly exact closed-form solutions to the Falkner–Skan boundary layer equation for varying wedge angle. This adds to the increasing number of problems in disparate areas of mathematical physics to which asymptotic approximants have been applied successfully (**12**–**17**). Advantages of asymptotic approximants, specifically for the Falkner–Skan problem and in general for other problems, are their simple form, ability to yield highly accurate solutions, accuracy in solution derivatives and low computational load. The approximant is used to determine the singularities in the complex plane that prescribe the radius of convergence of the power series solution to the Falkner–Skan equation for a large range of wedge angles. One limitation of the methodology provided here is that accurate values of the wall velocity gradient, κ, and asymptotic parameter, B, are needed to construct the approximant. As these are determined numerically in the present work, the approximants can only be utilized in post-processing once numerics are implemented. In an approximant generated for the Sakiadis boundary layer in a previous paper (**15**), however, it is possible to predict with high accuracy these parameters by a judicious choice in approximant coefficients. In the same paper, the approximant used here is applied to the Blasius problem to predict κ and B, but the precision does not approach that of existing benchmarks (**22**) since, unlike the Sakiadis problem, higher-order asymptotic behavior is not incorporated in the approximant. Although not reported here, reasonable estimates for κ and B can be predicted applying the approximant for $0 \leq \beta \leq 1$, but the prediction method fails for $\beta < 0$. That said, one may interpolate between the numerically obtained tabulated results given in the Supplementary Data to obtain fairly accurate values for κ and B for values of β not tabulated. Implementation of approximants in this manner makes them fully independent of further numerical predictions.

Supplementary data

Supplementary data are available online at *Quarterly Journal of Mechanics and Applied Mathematics*.

References

1. H. Schlichting, *Boundary Layer Theory*, 7th edn. (McGraw-Hill, New York, 1979).
2. T. Cebeci and H. B. Keller, Shooting and parallel shooting methods for solving the Falkner–Skan boundary-layer equation, *J. Comput. Phys.* **7** (1971) 289–300.
3. C. Laine and L. Reinhart, Further numerical methods for the Falkner–Skan equations: shooting and continuation techniques, *Int. J. Numer. Methods Fluids* **4** (1984) 833–852.
4. R. Fazio, A novel approach to the numerical solution of boundary value problems on infinite intervals, *SIAM J. Numer. Anal.* **33** (1996) 1473–1483.

5. A. Asaithambi, A finite-difference method for the Falkner–Skan equation, *Appl. Math. Comput.* **92** (1998) 135–141.

6. S. S. Motsa and P. Sibanda, An efficient numerical method for solving Falkner–Skan boundary layer flows, *Int. J. Numer. Methods Fluids* **69** (2012) 499–508.

7. R. Fazio. Blasius problem and Falkner–Skan model: Töpfer's algorithm and its extension. *Comput. Fluids* **73** (2013) 202–209.

8. C.-S. Liu. An iterative method based-on eigenfunctions and adjoint eigenfunctions for solving the Falkner–Skan equation. *Appl. Math. Lett.* **67** (2017) 33–39.

9. H. Bararnia, N. Haghparast, M. Miansari and A. Barari, Flow analysis for the Falkner–Skan wedge flow, *Curr. Sci.* **103** (2012) 169–177.

10. B. I. Yun, New approximate analytical solutions of the Falkner–Skan equation, *J. Appl. Math.* **2012** (2012) 1–12.

11. A. Khidir, A note on the solution of general Falkner–Skan problem by two novel semi-analytical techniques, *Propul. Power Res.* **4** (2015) 212–220.

12. N. S. Barlow, A. J. Schultz, S. J. Weinstein and D. A. Kofke, An asymptotically consistent approximant method with application to soft- and hard-sphere fluids, *J. Chem. Phys.* **137** (2012) 204102.

13. N. S. Barlow, A. J. Schultz, S. J. Weinstein and D. A. Kofke, Critical isotherms from virial series using asymptotically consistent approximants, *AIChE J.* **60** (2014) 3336–3349.

14. N. S. Barlow, A. J. Schultz, S. J. Weinstein and D. A. Kofke. Communication: analytic continuation of the virial series through the critical point using parametric approximants, *J. Chem. Phys.* **143** (2015) 1–5.

15. N. S. Barlow, C. R. Stanton, N Hill, S. J. Weinstein and A. G. Cio, On the summation of divergent, truncated, and underspecified power series via asymptotic approximants, *Q. J. Mech. Appl. Math.* **70** (2017) 21–48.

16. N. S. Barlow, S. J. Weinstein and J. A. Faber, An asymptotically consistent approximant for the equatorial bending angle of light due to Kerr black holes, *Class. Quant. Grav.* **34** (2017) 1–16.

17. R. J. Beachley, M. Mistysyn, J. A. Faber, S. J. Weinstein and N. S. Barlow, Accurate closed-form trajectories of light around a Kerr black hole using asymptotic approximants, *Class. Quant. Grav.* **35** (2018) 1–28.

18. C. M. Bender and S. A. Orszag, *Advanced Mathematical Methods for Scientists and Engineers I: Asymptotic Methods and Perturbation Theory* (McGraw-Hill, New York, 1978).

19. P. A. Frost and E. Y. Harper, An extended Padé procedure for constructing global approximations from asymptotic expansions: an explication with examples, *SIAM Rev.* **18** (1976) 62–91.

20. J. S. R. Chisholm, Generalisations of Padé approximants, *Circuits Syst. Signal Process* **1** (1982) 279.

21. G. A. Baker Jr. and P. Graves-Morris. *Padé Approximants*, 2nd edn. (Cambridge University Press, New York, 1996).

22. J. P. Boyd, The Blasius function: computations before computers, the value of tricks, undergraduate projects, and open research problems, *SIAM Rev.* **50** (2008) 791–804.

23. S. Anil Lal and M. Neeraj Paul, An accurate Taylor series solution with high radius of convergence for the Blasius function and parameters of asymptotic variation, *JAFM* **7** (2014) 557–564.

24. K. Stewartson, Further solutions of the Falkner–Skan equation, *Proc. R. Philos. Soc.* **50** (1954) 454–465.

25. P. L. Sachdev, R. B. Kudenatti and N. M. Bujurke, Exact analytic solution of a boundary value problem for the Falkner–Skan equation, *Stud. Appl. Math*. **120** (2008) 1–16.
26. W. A. Coppel, On a differential equation of boundary layer theory, *Philos. Trans. R. Soc. Lond. A* **253** (1960) 101–136.
27. R. V. Churchill, *Complex Variables* (McGraw-Hill, New York, 1948).
28. P. Gonnet, S. Güttel and L. N. Trefethen, Robust Padé approximation via SVD, *SIAM Rev.* **55** (2013) 101–117.
29. G. A. Baker Jr. and J. L. Gammel, The Padé approximant, *J. Math. Anal. Appl.*, **2** (1961) 21–30.
30. E. C. Titchmarsh, *The Theory of Functions*, 2nd edn. (Oxford University Press, 1968).
31. M. Van Dyke, *Perturbation Methods in Fluid Mechanics* (Parabolic, Stanford, Calif., 1975).
32. A. J. Guttmann and I. Jensen, Series analysis, *Polygons, Polyominoes, and Polycubes* (ed. A. J. Guttmann, Springer, Dordrectht, The Netherlands, 2009) 181–202.
33. J. P. Boyd, The Blasius function in the complex plane, *Exp. Math.* **8** (1999) 381–394.